PNAS
www.pnas.org

Supplementary Information for

Phosphoregulated FMRP Phase Separation Models Activity-Dependent Translation through Bidirectional Control of mRNA Granule Formation

Brian Tsang, Jason Arsenault, Robert M. Vernon, Hong Lin, Nahum Sonenberg*, Lu-Yang Wang, Alaji Bah* and Julie D. Forman-Kay*

Julie D. Forman-Kay
Email: forman@sickkids.ca

Alaji Bah
Email: baha@upstate.edu

Nahum Sonenberg
Email: nahum.sonenberg@mcgill.ca

This PDF file includes:

www.pnas.org/cgi/doi/10.1073/pnas.1814385116

Supplementary Information Text

SI Materials and Methods

Protein Expression and Purification. $FMRP_{LCR}$,(1) $FMRP_{LCR}$(RtoK)(1) and 4E-BP2(2) were expressed and purified as previously described. Full-length human cDNA FMRP was generated by gene synthesis (GenScript) and subcloned into a pET-SUMO Vector (Invitrogen). Using the pET-SUMO-FMRP plasmid as a template, $FMRP_{\Delta LCR}$ was generated via QuikChange Site-Directed Mutagenesis (Agilent) by inserting a TAG stop codon after Threonine 455 of full-length FMRP. The constructs were transformed into *Escherichia coli* BL21 (DE3) Codon Plus Cells (Agilent) and grown at 37°C in Lennox broth medium. Protein expression was induced with 0.2 mM isopropyl-β-D-thiogalactopyranoside (IPTG) at an optical density (600 nm) of ~ 0.6, followed by ~18 hours of additional growth at 16°C. Cells were harvested by centrifugation and pellets stored at -20°C.

Pellets containing His-SUMO-FMRP or His-SUMO-$FMRP_{\Delta LCR}$ fusions were re-suspended in lysis buffer containing 50 mM Tris, pH 8.0, 150 mM NaCl, 20 mM imidazole, 10% Glycerol, 250 mM arginine, 5 mM benzamidine and 2 mM of dithiothreitol (DTT), supplemented with DNAse 1 and complete protease inhibitor tablet (Sigma-Aldrich). After cell lysis via sonication and centrifugation, the filtered supernatant was loaded onto a 5 mL HisTrap HP column (GE Healthcare) equilibrated in the same lysis buffer. The column was extensively washed with 20-column volumes (CV) of the same buffer supplemented with 50 mM imidazole. SUMO-fusion proteins were eluted using a 100-500 mM imidazole gradient, and protein-containing fractions were combined. The combined fractions were passed through a 0.2 µm filter to separate any aggregated products. A hexa-histidine tagged Ulp protease was added to cleave off the His-SUMO tag overnight at ~ 8°C (cold room) while dialyzing against 4 liters of 50 mM Tris pH 8.0, 250 mM NaCl, 20 mM imidazole, 10% glycerol, 250 mM arginine, 5mM benzamidine, 1 mM EDTA and 2 mM DTT. After dialysis, the protein solution was passed through a 0.2 µm filter again to separate any aggregated products. Uniform completion of the Ulp cleavage reaction was confirmed by SDS-PAGE. The protein of interest was separated from the hexa-histidine tagged Ulp protease and His-SUMO by passing the reaction over a 5 mL HisTrap HP column for a second time equilibrated in the same dialysis buffer. Flow-through and wash fractions (lysis buffer supplemented with 50 mM imidazole) that contain the protein of interest were combined and then loaded onto a Superdex 200 gel filtration column (GE Healthcare) pre-equilibrated with the same lysis buffer.

The purified proteins were dialyzed three times in desired buffers. Protein purity was analyzed by both SDS-PAGE and mass spectrometry, while protein concentrations were determined by absorbance at 280 nm using a molar extinction coefficient of 48360 $M^{-1}cm$ for full-length FMRP and 38390 $M^{-1}cm$ for $FMRP_{\Delta LCR}$. The UV absorbance ratio of 260/280 nm < 0.6 was used to verify that there is no RNA contamination for purified protein samples.

Live Cell Experiments and Imaging. A SacI restriction site was introduced into a plasmid vector(3) containing the cDNA of Isoform1 of FMRP, directly upstream of the start codon, using QuikChange II Site-directed mutagenesis kit (Agilent). The full FMRP isoform 1 cDNA was cut out with restriction enzymes SacI and SalI, and then inserted into a pCFP-N1 vector (Addgene) using T4 ligase (New England Biolabs). To generate a contiguous FMRP-CFP reading frame, the FMRP stop codon was suppressed by a single point mutation using Site-Directed mutagenesis using QuikChange Site-Directed

Mutagenesis (Agilent). The integrity of the FMRP-CFP plasmid was confirmed by DNA sequencing.

CHO cells were grown at 37°C (5 % CO_2) in F-12K Nutrient Mixture (Gibco) supplemented with 1% Pen/Strep (10 000 U/ml; Thermo Fisher Scientific) and 10% Fetal Bovine Serum (HyClone). Cells were seeded at $1x10^5$ cells per well inside 30 mm glass bottom culture dishes (MatTek). 24 hrs after plating, the cells were transfected with 2.4 µg of CFP or FMRP-CFP plasmid DNA using Lipofectamine 3000 (Thermo Fisher Scientific) following manufacturer's protocol. 48 hrs after transfection, DiI (Thermo Fisher Scientific), dissolved at 2 mg/mL in DMSO (Sigma-Aldrich), was added to the dish at 2 µg/mL final concentration and Hoechst 33342 (Invitrogen) was added at 1:1000 final concentration in the culture medium. Cells were incubated at 37°C for 30 min. Images were taken on a Quorum Spinning Disk Confocal (Olympus IX81) using a 60x/1.35 (Oil immersion) lens and a Hamamatsu C9100-13 EM-CCD camera. Blue CFP channel was excited using a 405 nm (50 mW) laser and observed with a 447/40 emission filter wheel. Red DiI channel was excited using a 561 (50 mW) laser and observed with a 624/40 emission filter wheel (shown as yellow in figures for better visual contrast). Z-stacks were taken at 0.5 µm intervals. Images were processed using the Volocity program (Perkin-Elmer) and formatted for publication using ImageJ.

Fluorescent Protein Labeling and Purification. $FMRP_{LCR}$ has a natural cysteine at position 584 and 4E-BP2 has two natural cysteines, one at position 35 and another at position 73. Both purified proteins were dialyzed into labeling buffer containing 50 mM Tris pH 7.5, 150 mM NaCl and 4 M GdmCl and labeled with 5X Cy3 or Cy5 mono-maleimide dye (Lumiprobe) according to manufacturer's instruction. All reactions were incubated overnight at 4°C degrees and quenched with excess DTT the following day. Unreacted fluorophores were removed by first dialysis and then with de-salting using a 5 mL HiTrap desalting column (GE healthcare) equilibrated with dialysis buffer. Protein fractions were collected and final concentrations were measured with A280 nm absorbance. Labeling efficiency was determined with mass spectrometry by comparing the additional mass of each fluorophore compared to the mass of non-labeled protein.

FRAP Method and Analysis. Fluorescence recovery after photobleaching experiments were performed on a Leica DMI6000 SP8 Confocal microscope with a 63x/1.4 oil objective using a Hamamatsu C9100-13 EM-CCD camera. A $FMRP_{LCR}$-sc1 RNA sample was produced with 150 µM Cy5-tagged $FMRP_{LCR}$ mixed with 5 µM Cy3-tagged sc1 RNA (final concentrations) in a buffer containing 25 mM Na_2PO_4 pH 7.4, 30 mM NaCl, 2 mM DTT. The sample was bleached for 0.68 seconds (1 pulse) with 95% laser power at 522 nm for Cy3-sc1 or at 649 nm for Cy5-$FMRP_{LCR}$. A single confocal plane was maintained and imaged throughout the FRAP experiment. Recovery of a ~1 µm diameter bleached region within a droplet was recorded for 120 seconds at 1% laser power to mitigate photobleaching due to imaging. The recovery intensities were corrected for overall background photobleaching during image acquisition (using intensities from a non-bleached droplet), normalized to the same prebleach spot intensity and fitted to a single exponential function. Images were processed on Volocity (Perkin-Elmer) and ImageJ (NIH).

Preparation of Condensed Phase-separated $FMRP_{LCR}$ for NMR Spectroscopy. Typically, a condensed phase sample requires ~200 mg of $FMRP_{LCR}$ protein and ~15% of that is ^{15}N,^{13}C isotopically labeled. Phase separation was induced by dialysis in the cold room of a highly concentrated solution (~2.5 mL in volume) of $FMRP_{LCR}$ in 50 mM Tris pH 8.0, 150 mM NaCl, 2M guanidinium chloride (GdmCl) and 5 mM TCEP into a

buffer containing 10 mM Na_2PO_4 pH 7.4 and 5 mM TCEP. Dialysis was completed using a 3.5kDa MWCO MAXI GeBAflex-tube and at least two dialyses were performed against 4L of buffer to ensure complete removal of GdmCl. During dialysis, ~ 2 - 3 mM $FMRP_{LCR}$ solution phase separates into small liquid droplets resulting in a cloudy solution. Concentrated samples were incubated on ice to form a two-phase system which is used to verify that enough condensed protein sample is formed. Afterwards, the solution is disrupted via vortexing vigorously reforming a turbid mixture. Upon transfer of the turbid solution to a 5-mm Shigemi NMR tube placed on ice, $FMRP_{LCR}$ droplets gradually coalesce to reform a distinct two phase system: a dilute monomeric state (top) and condensed phase-separated state (bottom) with concentrations of 0.25 mM (5.1 mg/mL) and 10.2 mM (210 mg/mL), respectively, at 5°C as determined by 280 nm absorbance reading.

NMR Spectroscopy. Isotopically enriched $FMRP_{LCR}$ was grown in M9 minimal media containing $^{15}NH_4Cl$ (Cambridge Isotope Labs) and ^{13}C glucose (Cambridge Isotope Labs). Purification was performed as described above. 2D-^{1}H-^{15}N heteronuclear single-quantum coherence (HSQC) experiments were performed on a Varian INOVA 600 MHz NMR spectrometer equipped with pulsed field gradient units and triple resonance probes. When collecting the NMR data for the phase-separated state, it is critical to ensure that the amount of condensed phase-separated material in the NMR tube was more than enough to occupy the whole volume of the NMR coil. NMR experiments were done at 5 °C and processed with the NMRPipe software package(4) and NMR spectra analyzed using SPARKY.

***In vitro* Partitioning Assay.** 250 µM of $FMRP_{LCR}$ was mixed with 5 µM of sc1 RNA and 500 nM of Cy3-labeled molecule (Cy3 dye, BSA, 4E-BP2, sc1-RNA, miRNA-125b). Experiments were performed in buffer containing 25 mM Na_2PO_4 pH 7.4 and 2 mM DTT. After incubation on ice for 30 minutes, the mixture was spun down at 21,000 g for 10 minutes at 4 °C resulting in a bulk two-phase partitioned system, with the protein-depleted phase on top and a small protein condensed phase at the bottom. The remaining Cy3 concentration from the protein-depleted phase was compared against the total Cy3 concentration (before phase separation). Cy3 concentrations were determined by measuring its absorbance at 552 nM with an extinction coefficient of 0.15 $\mu M^{-1}cm^{-1}$.

DIC and Fluorescence Microscopy of Phase Separated Samples. Microscopy of phase-separated droplets was performed by mixing protein in 25 mM Na_2PO_4 pH 7.4, 30 mM KCl, 2 mM TCEP with desired RNA in TE buffer in a (1:1) mixture to achieve desired concentrations. The protein-RNA solution was thoroughly mixed and incubated on ice for ~5 minutes (or until visibly turbid), following which 10 µL of the protein-RNA mixture was transferred onto a 35 mm glass bottom dish (MatTek) or onto a 96 glass well plate (Eppendorf) for immediate imagining. Differential interference contrast (DIC) and fluorescence images were obtained on an Axio Observer 7 bright field and fluorescence inverted microscope (Carl Zeiss) with either 40X (air) or 63X objective (air) using an Axiocam 702 mono CMOS camera. The presence or absence of droplet formation in different conditions (phase separation) is defined here by DIC observation of round droplets with greater or equal to 1 µm diameter. All images represent a single focal plane focused onto the surface of the glass slide. Images were processed with Volocity (Perkin-Elmer) and ImageJ (NIH).

Quantification of the Partition Coefficient. Fluorescence images of $FMRP_{LCR}$-Sc1 RNA droplets with the addition of Cy3 labeled molecules (dye, BSA, sc1 RNA, miR-

125b, or 4E-BP2) were acquired as described above and analyzed using ImageJ. Only droplets settled onto the focal plane of the coverslip was used for the analysis. Background artifacts were corrected for by subtracting an image of buffer alone. Masks were defined using the Otsu threshold method and only droplets with a radius between 1 - 5 μm and with a circularity of 0.5-1.0 were selected using the particle picking algorithm in ImageJ. The intensity of the bulk background solution was defined as the mean intensity within a circular ROI with a diameter of 5 μm that does not contain any fluorescence particles. Partition coefficients were calculated from the ratio of mean fluorescence intensity (droplet) / mean fluorescence intensity (bulk background solution) +/- standard deviation from three measurements across three random slides.

Phosphorylation and Methylation of Protein. Casein Kinase II (CK2) phosphorylation of $FMRP_{LCR}$ (phospho-$FMRP_{LCR}$) was performed on purified $FMRP_{LCR}$ using a previously described dialysis technique (5). 5 μL of CKII (New England Biolabs) was mixed with 5 mL of ~100 μM $FMRP_{LCR}$ in phosphorylation buffer containing 20 mM Tris pH 7.4, 10 mM $MgCl_2$, 4 mM ATP, 0.5 mM EGTA and 2 mM DTT. The reaction was dialyzed against 4 L of the same phosphorylation buffer overnight at room temperature (~20 hours or until desired phosphorylation state is achieved). Mass spectrometric analysis was used to determine the degree of phosphorylation and concentrated guanidinium chloride solution was added to stop the reaction once the desired phosphorylation state was reached. Afterwards, the quenched reaction mixture was concentrated and passed over a Superdex 75 gel filtration column (GE healthcare) equilibrated with 20 mM Tris pH 8.0, 4M GdmCl,150 mM NaCl, 2 mM DTT. Gel filtration fractions containing phosphorylated protein were pooled, concentrated and dialyzed into appropriate buffers for downstream assays.

Methylation of $FMRP_{LCR}$ (Me-$FMRP_{LCR}$) by Protein Arginine N-methyltransferase1 (PRMT1) was generated by co-transfecting *Escherichia coli* BL21 (DE3) Codon Plus cells with pET SUMO-$FMRP_{LCR}$ plasmid containing a kanamycin resistance marker and a pGEX-PRMT1 plasmid containing an ampicillin resistance marker. Colonies containing both plasmids were selected on LB-agar plates mixed with both kanamycin and ampicillin. Purification of Me-$FMRP_{LCR}$ follows the method described for $FMRP_{LCR}$ and methylation efficiency was determined with mass spectrometry of purified samples.

Binding Assay using Fluorescence Polarization (FP). 5' labeled 6-FAM sc1 RNA was reconstituted in TE buffer and frozen at -20°C. For FP binding assays, increasing concentrations of $FMRP_{LCR}$, Me-$FMRP_{LCR}$, or RtoK-$FMRP_{LCR}$ in reaction buffer containing 25 mM Na_2PO_4, pH 7.4, 50 mM KCl, 2 mM DTT, 0.02 mg/mL *E.* coli tRNA (Sigma) and 0.01% NP-40 (Sigma) were mixed (1:1; v/v) into a constant 6-FAM sc1 RNA concentration (50 nM diluted from 100 μM TE stock in reaction buffer). The sc1 RNA was heated to 90°C for 5 minutes and then cooled to room temperature before mixing with FMRP (1:1 v/v resulting in a final RNA concentration of 25 nM with varying protein concentrations). The reaction mixture was equilibrated at room temperature for at least 3 hours. Apparent fluorescence polarization was monitored in a 384-well plate (3820 Corning) with a SpectraMax i3x Multi-Mode Plate Reader (Molecular Devices) at 25°C. For each experiment, the values of three reads were averaged. Average values and standard deviation from three independent replicate experiments were calculated and plotted against each protein concentration. Apparent dissociation constants ($K_{d,app}$) were obtained by fitting the data using a Hill plot binding model (eq. 2).

$$Fp = \frac{maxFP * [FMRP]^h}{Kd_{app}^h + [FMRP]^h} \qquad (eq. 2)$$

***In vitro* Translation Assay.** *In vitro* translation of luciferase mRNA (Promega) was performed with nuclease treated Rabbit Reticulocyte Lysate System (Promega). When opening the kit for the first time, all provided batches of lysates were pooled together, mixed and aliquoted evenly to ensure reproducible results in the translation assay. Reactions were carried out according to manufacturer protocol with slight modifications. A 1X (30 µL) reaction contains 12.6 µL of rabbit reticulocyte lysate, 0.5 µL of Luciferase mRNA (1 mg/mL), 0.3 µL of amino acid mixture minus leucine (1 mM), 0.3 µL of amino acid mixture minus methionine (1 mM), and 16.3 µL of protein, puromycin (Sigma) or buffer (25 mM $NaPO_4$ pH = 7.4, 50 mM KCl, 2 mM DTT). All *in vitro* translation reactions were prepared on ice and then incubated at room temperature for 3 hours before luminescence measurement.

Translation of luciferase was directly monitored using a standard luciferase assay system (Promega). The provided luciferase substrate was prepared according to manufacturer instructions. A standard reaction contained 75 µL of luciferase substrate mixed with 2 µL of unpurified translation mixture in a white opaque 96 well plate (Corning 3990). End-point luminescence measurements were carried out using a SpectraMax i3x Multi-Mode Plate Reader (Molecular Devices) at 25°C. Luminescence measurements represent mean values obtained from two independent *in vitro* translation reactions, each of them measured three times. Curve fitting of the data was performed using GraphPad Prism, using the built-in dose-response model with a variable slope. The unpurified translation assay mixtures with different components, or rabbit reticulocyte lysates, were directly transferred onto a glass slide after mixing and visualized for the appearance of liquid droplets with DIC microscopy (as described above).

Bioinformatics Assessment. In order to identify proteins with general function across diverse cellular RNA granules, we took the core RNA granule proteome from Bio-ID interaction(6) and used the full list of significant interaction hits to identify all interactions between proteins in the core RNA granule proteome. For this analysis, interaction sets are defined for each protein as "prey", and a positive interaction requires a significant enrichment observed to any "bait" protein, without requiring enrichment to both the N- and C-terminal baits. Granule identities were taken from the NPF definitions in the dataset, and highly general RNA granule proteins were determined by taking the top third of the proteome by the total number of interactions involving each protein. We confirm in all cases that this captures proteins with interactions to proteins found in stress granules, P-bodies, and other RNA granules (RNPs), rather than a high number of interactions to a single granule type (Table S1). Functional roles in translation inhibition were taken from the gene ontology database using AmiGO2 version 2.4.26, database release date 2017-07-05, GO term GO: 0017148 (negative regulation of translation)(7, 8), and predictions for involvement in phase separation were taken from previously reported phase separation prediction values based on long-range pi-pi interactions(1)

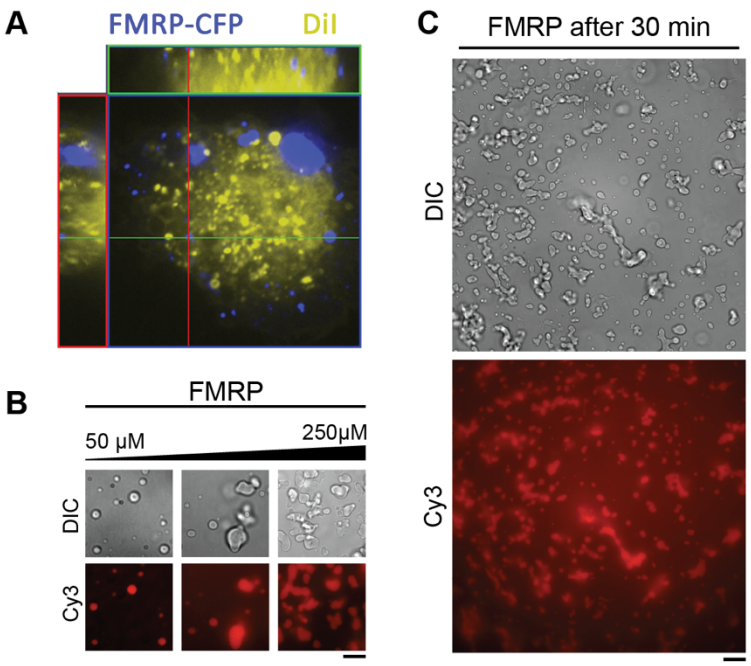

Figure S1. FMRP foci do not colocalize with DiI in CHO cells and concentrated full-length FMRP forms non-spherical higher-order assemblies *in vitro*.
(A) Orthogonal views of a CHO cell transfected with FMRP-CFP (blue) and stained with DiI (yellow). FMRP-CFP fluorescence is punctate and predominantly does not colocalize with DiI (lipid stain). **(B)** Representative images of increasing FMRP concentration from 50 to 250 μM (25 mM Na_2PO_4, pH 7.4, 30 mM NaCl, 2 mM DTT) in the presence of Cy3-labeled sc1 RNA (5 μM) at room temperature, showing spherical droplets at the lower FMRP concentration and non-spherical gel-like assemblies enriched with sc1 RNA at the higher concentrations. Scale bar represents 10 μm. **(C)** Representative images of 50 μM FMRP mixed with Cy3-sc1 RNA after 30 minutes of incubation on ice (same conditions as (B)). Gel-like assemblies stick together with non-spherical morphology. Scale bar represents 10 μm.

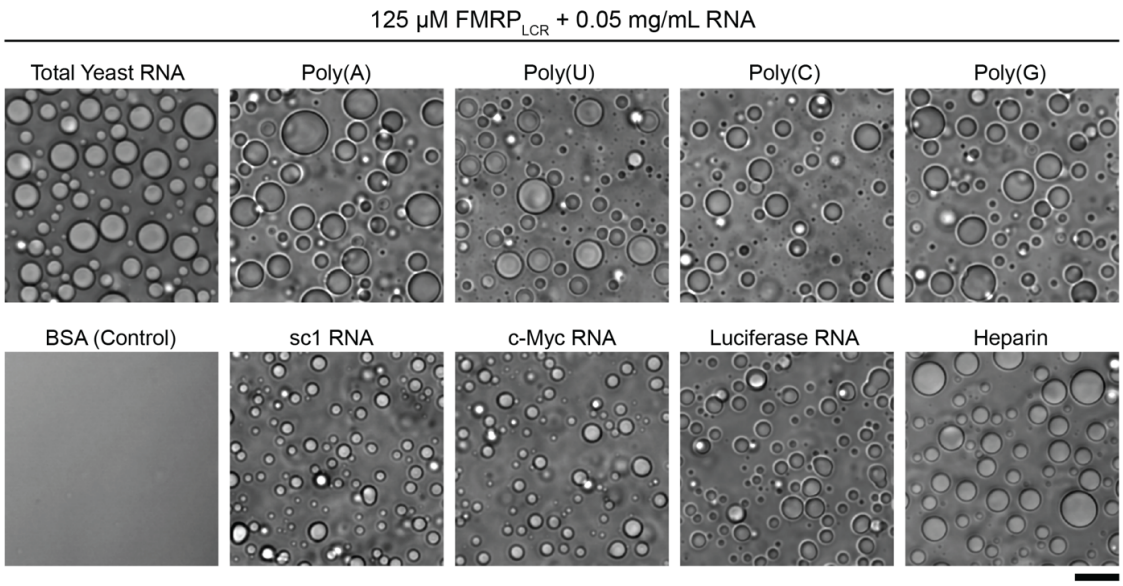

Figure S2. FMRP$_{LCR}$:RNA phase separation is not dependent on RNA sequence or structure but is likely driven by protein:RNA electrostatic and pi-pi interactions.

Representative DIC microscopy images of different RNAs or BSA (0.05 mg/mL) mixed with FMRP$_{LCR}$ (125 μM final concentration) in buffer containing 25 mM Na_2PO_4 pH 7.4, 30 mM NaCl, 2 mM DTT. All tested species induced droplet formation, including heparin, a polyanionic polymer.

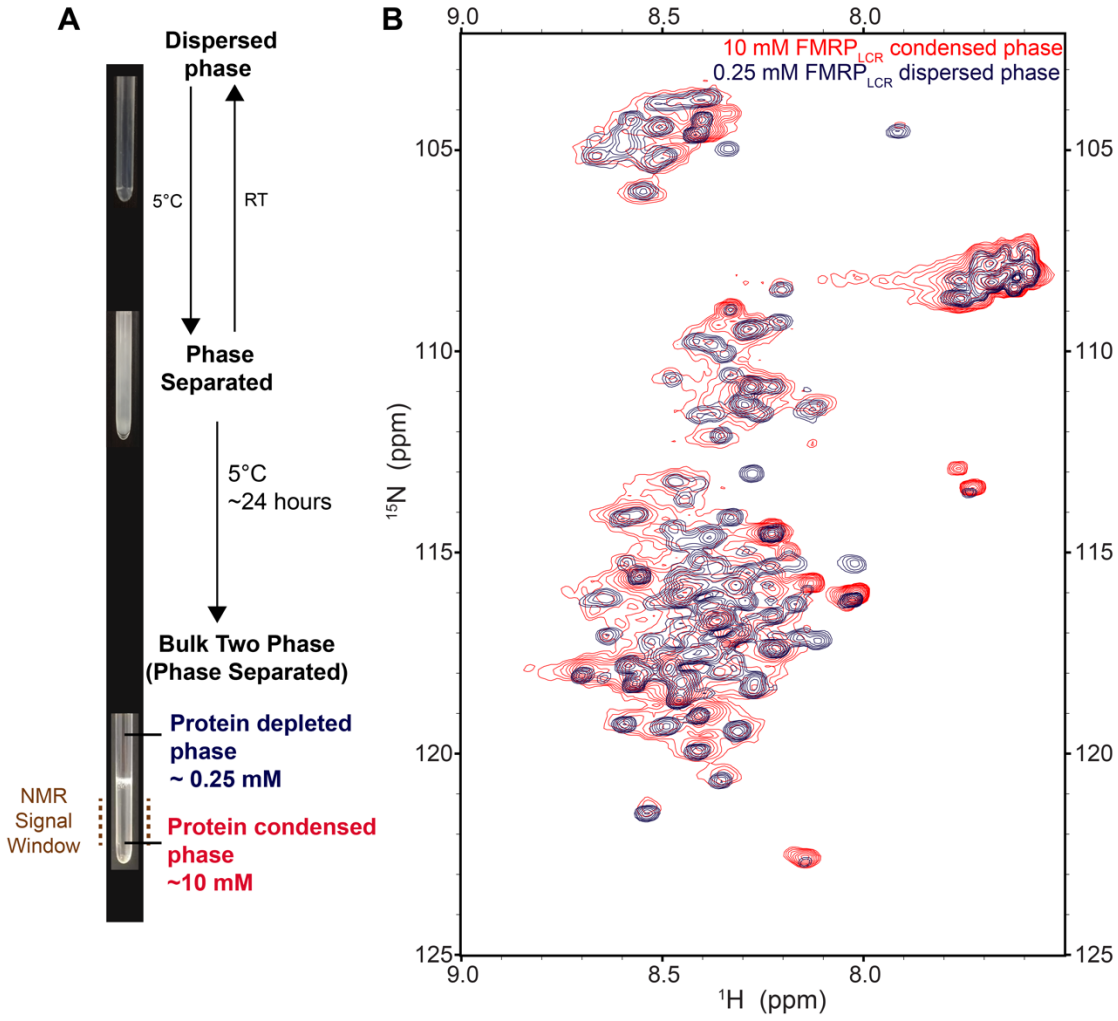

Figure S3. FMRP$_{LCR}$ is structurally disordered in both dispersed (monomer) and condensed (phase-separated) states.
(A) Outline of the procedure used to produce FMRP$_{LCR}$ dispersed and condensed NMR samples. Concentrations were measured by manually pipetting and diluting either the isolated protein-depleted or protein-condensed phase from the same sample into a buffer and then measuring absorbance at 280 nm. The final bulk two-phase picture is zoomed in to show the phases clearly, and some of the protein-depleted phase has been removed by pipetting. **(B)** Overlay of ^{1}H-^{15}N heteronuclear single quantum coherence (HSQC) spectra of FMRP$_{LCR}$ dispersed and condensed phase samples. A similarly narrow chemical shift dispersion for both samples implies a similar global disordered conformation in both states.

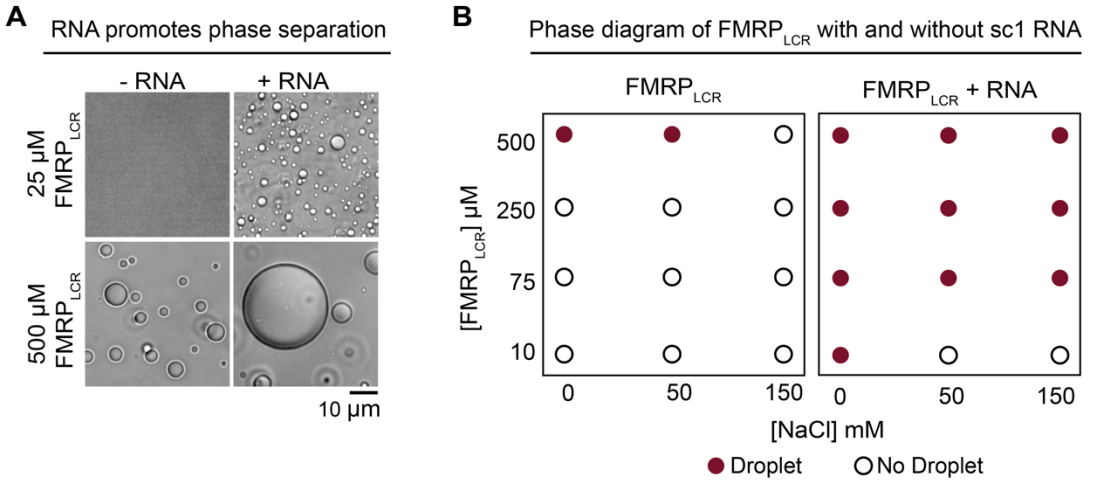

sc1 RNA (36-nt) sequence: r(GCUGCGGUGUGGAAGGAGUGGUCGGGUUGCGCAGCG)

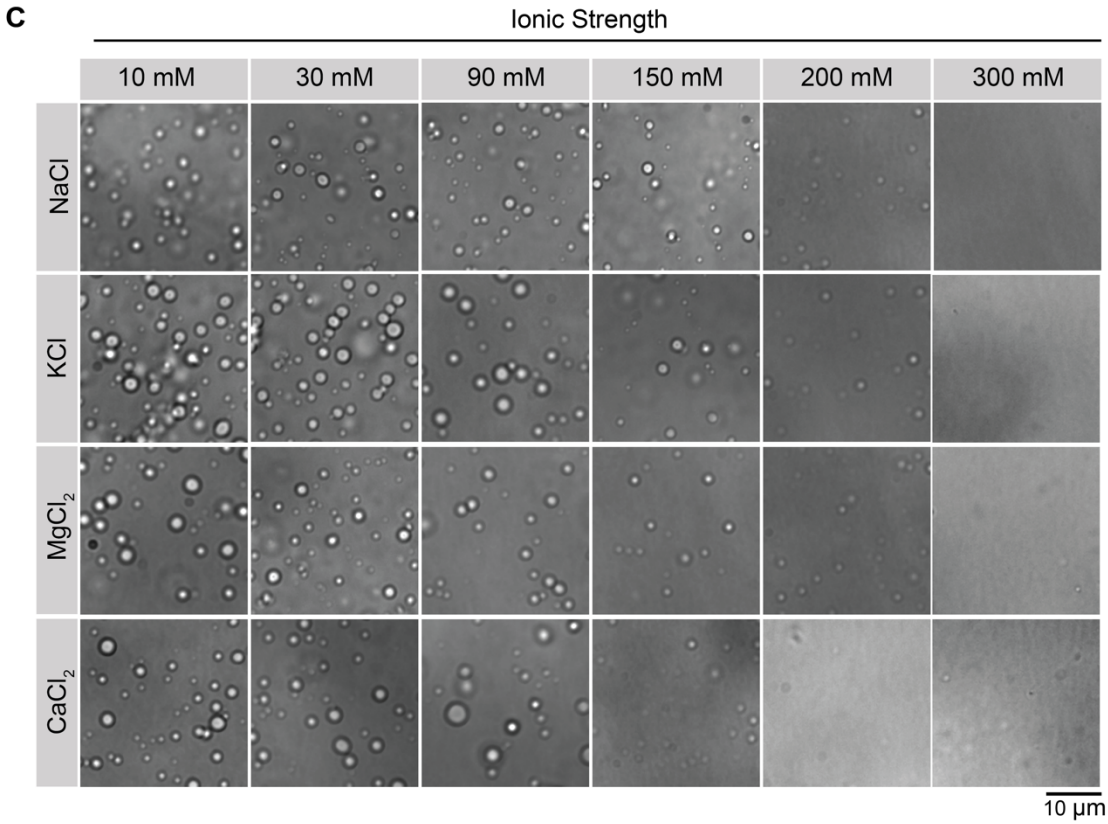

$$\mathrm{I} = \frac{1}{2}\sum_{i=1}^{n} c_i\, z_i^2 \quad \textbf{(eq. 1)}$$

I = ionic strength (mM); C = molar concentration of ion i (mM); Z = charge of ion i

Figure S4. Addition of sc1 RNA promotes FMRP$_{LCR}$ phase separation while the addition of different salt ions perturbs it.
(A) DIC microscopy images of FMRP$_{LCR}$ at 25 μM or 500 μM with or without 5 μM sc1 RNA (sequence shown below) in buffer containing 10 mM Na_2PO_4, pH 7.4, 2

mM DTT. Addition of RNA increases phase separation propensity by ~20-fold. **(B)** Phase diagrams of $FMRP_{LCR}$ and $FMRP_{LCR}$ at varying concentrations with sc1 RNA at 5 μM RNA constructed based on observations of droplet formation. Red circles indicate droplet detection and open circles indicate no droplet detection. **(C)** DIC images of $FMRP_{LCR}$ at identical concentrations of 100 μM protein with 2.5 μM sc1 RNA (25 μM Na_2PO_4 pH 7.4, 30 mM NaCl 2 mM DTT) but treated with different ions with varying valences (at room temperature). No crowding reagents were used. Salt concentrations were adjusted such that the same ionic strength is achieved according to equation 2. While some differences might exist between different ions, in general, similar ionic strengths lead to similar effects on droplet assembly.

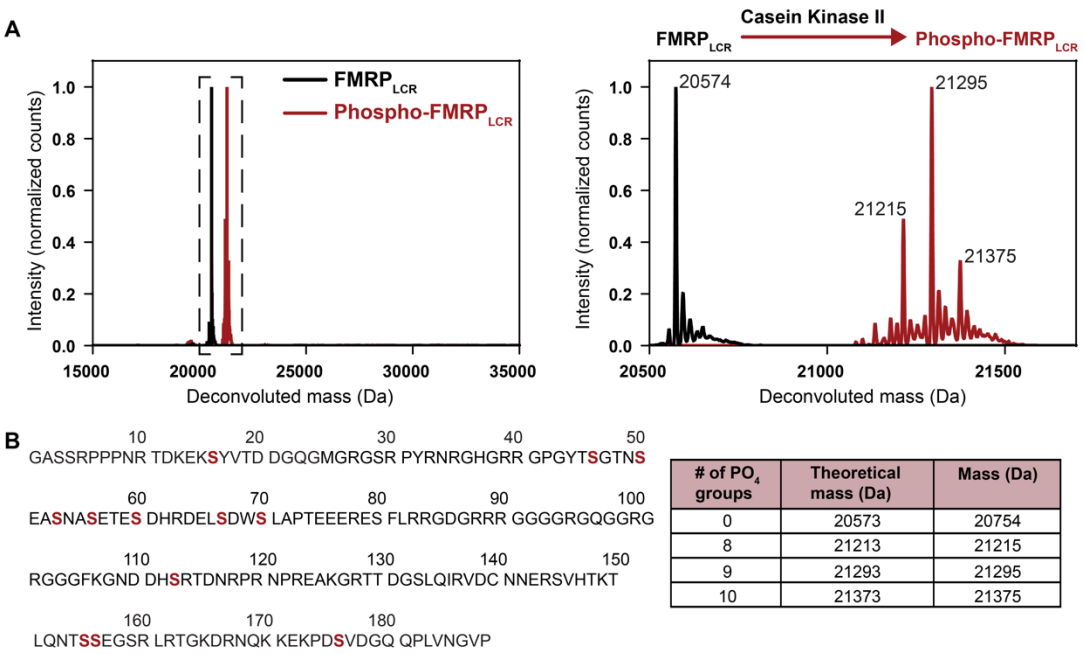

# of PO_4 groups	Theoretical mass (Da)	Mass (Da)
0	20573	20754
8	21213	21215
9	21293	21295
10	21373	21375

Figure S5. Representative mass-spectrometric analysis of phosphorylated FMRP$_{LCR}$ by casein kinase II.
(A) (left) Electrospray ionization mass spectrometry analysis of FMRP$_{LCR}$ (black) overlaid with phospho-FMRP$_{LCR}$ (red). **(right)** Zoomed in spectra showing three distinct species corresponding to the addition of 8 to 10 phosphate groups. **(B)** Serine residues that fit the CKII sequence motif (SX$_{1-5}$E/D) are highlighted in red.

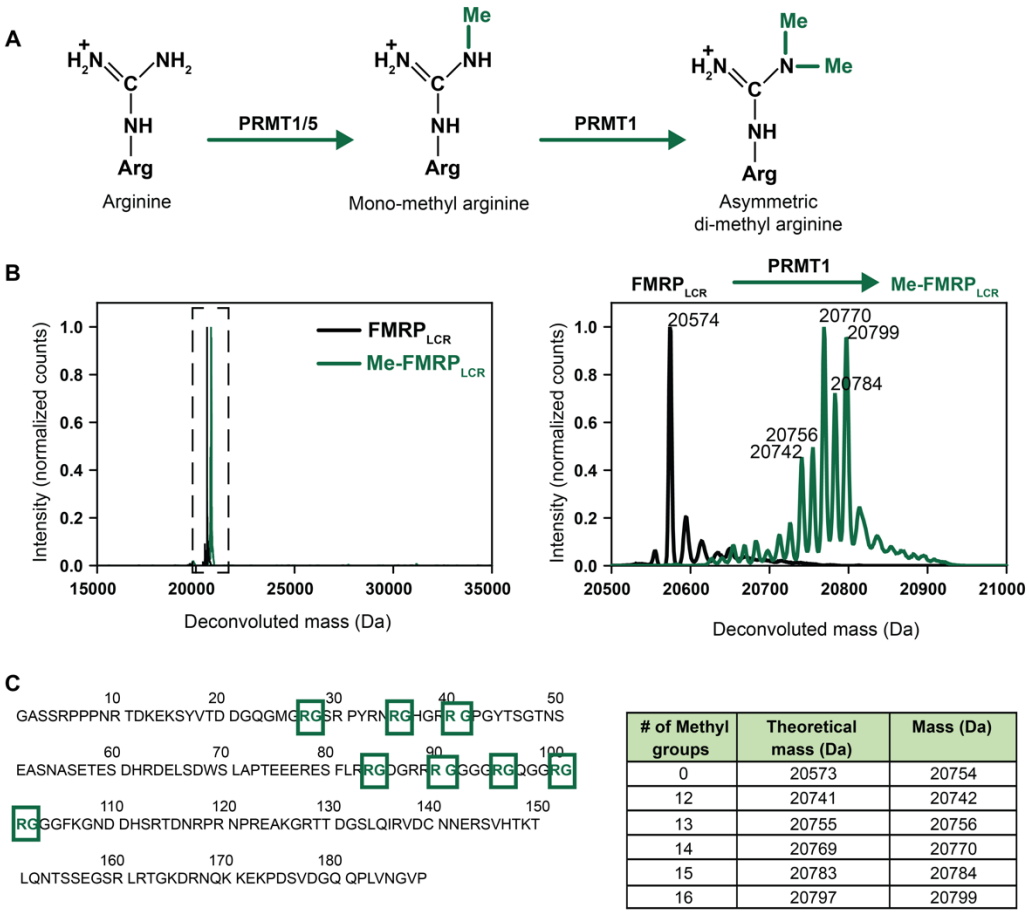

# of Methyl groups	Theoretical mass (Da)	Mass (Da)
0	20573	20754
12	20741	20742
13	20755	20756
14	20769	20770
15	20783	20784
16	20797	20799

Figure S6. Representative mass-spectrometric analysis of methylated $FMRP_{LCR}$ by PRMT1.
(A) Schematic depicting PRMT1-mediated asymmetric di-methylation of arginine. **(V) (left)** Electrospray ionization mass spectrometry analysis of $FMRP_{LCR}$ (black) overlaid with Me-$FMRP_{LCR}$ (green). **(right)** Zoomed in spectra showing five distinct species likely corresponding to the addition of 12-16 methyl groups. **(C)** Possible PRMT1 catalyzed methylation RG sites within the $FMRP_{LCR}$ sequence are highlighted and boxed in green. Asymmetric di-methylation of all 8 RG sites represents the addition of 16 methyl groups.

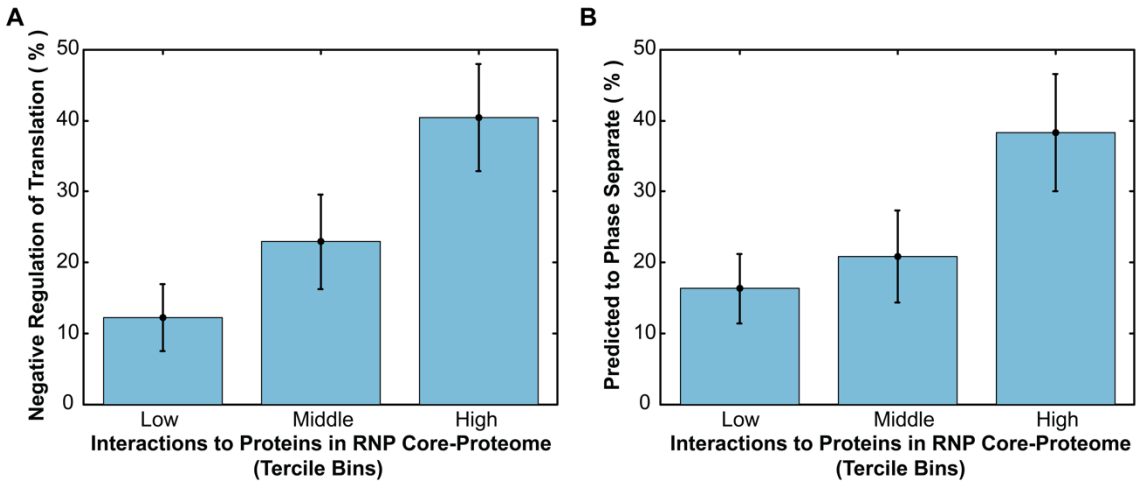

Figure S7. Analysis of core RNA granule proteome.
The set of 144 proteins in the core RNA granule proteome is divided into thirds (n=48) by ranking proteins by their overall promiscuity of interactions with other proteins in the data set, as described in the methods. **(A)** Highly promiscuous RNA granule proteins are more likely to be involved in negative regulation of translation. **(B)** Highly promiscuous RNA granule proteins are more likely to be predicted to phase separate. Error bars represent the standard error of the mean, as determined by bootstrap analysis.

Table S1. List of selected synaptic plasticity-associated RNA granule interacting proteins annotated as translational repressors and predicted, or demonstrated, to phase separate.

Gene	Protein Name	Functional Roles	Phase Separation
Caprin1	Caprin-1	Caprin is an RNA-binding protein strongly implicated in the control of local mRNA localization, which is required for synaptic plasticity and long-term memory formation(9). Heterozygous Caprin-1 knockout mice result in a reduction in social interaction behaviors, which is implicated in autism spectrum disorders(10).	Predicted(1)
CPEB4	Cytoplasmic polyadenylation element-binding protein 4	The CPEB family is involved in the regulation of translation(11) affecting learning and memory(12).	Experimental evidence(13)
GIGYF2	GRB10-interacting GYF protein 2	GIGYF2 is involved with IFG-1 signaling, which functions as a modulator for normal synaptic plasticity(14). GIGYF2 represses mRNA translation of mRNAs important for embryonic development(15).	Predicted(1)
FMR1	FMRP or Synaptic functional regulator FMR1	Loss of FMRP function results in defects in translational regulation(16) and cognitive deficits in multiple animal models(17).	Experimental evidence presented previously(1, 18) and here
FXR2	Fragile X mental retardation syndrome-related protein 2	FXR2P knockout mice have altered synaptic plasticity(19) along with impaired learning(20).	Predicted(1)

References

1. Vernon RM, et al. (2018) Pi-Pi contacts are an overlooked protein feature relevant to phase separation. *Elife* 7:e31486.
2. Lukhele S, Bah A, Lin H, Sonenberg N, Forman-Kay JD (2013) Interaction of the eukaryotic initiation factor 4E with 4E-BP2 at a dynamic bipartite interface. *Structure* 21(12):2186–96.
3. Arsenault J, et al. (2016) FMRP Expression Levels in Mouse Central Nervous System Neurons Determine Behavioral Phenotype. *Hum Gene Ther* 27(12):982–996.
4. Delaglio F, et al. (1995) NMRPipe: a multidimensional spectral processing system based on UNIX pipes. *J Biomol NMR* 6(3):277–93.
5. Bah A, et al. (2015) Folding of an intrinsically disordered protein by phosphorylation as a regulatory switch. *Nature* 519(7541):106–109.
6. Youn J-Y, et al. (2018) High-Density Proximity Mapping Reveals the Subcellular Organization of mRNA-Associated Granules and Bodies. *Mol Cell* 69(3):517–532.e11.
7. Ashburner M, et al. (2000) Gene Ontology: tool for the unification of biology. *Nat Genet* 25(1):25–29.
8. Expansion of the Gene Ontology knowledgebase and resources (2017) *Nucleic Acids Res* 45(D1):D331–D338.
9. Nakayama K, et al. (2017) RNG105/caprin1, an RNA granule protein for dendritic mRNA localization, is essential for long-term memory formation. *Elife* 6:e29677.
10. Ohashi R, Takao K, Miyakawa T, Shiina N (2016) Comprehensive behavioral analysis of RNG105 (Caprin1) heterozygous mice: Reduced social interaction and attenuated response to novelty. *Sci Rep* 6(1):20775.
11. Costa-Mattioli M, Sossin WS, Klann E, Sonenberg N (2009) Translational control of long-lasting synaptic plasticity and memory. *Neuron* 61(1):10–26.
12. Lu W-H, Yeh N-H, Huang Correspondence Y-S, Huang Y-S (2017) CPEB2 Activates GRASP1 mRNA Translation and Promotes AMPA Receptor Surface Expression, Long-Term Potentiation, and Memory. *Cell Rep* 21:1783–1794.
13. Guillén-Boixet J, Buzon V, Salvatella X, Méndez R (2016) CPEB4 is regulated during cell cycle by ERK2/Cdk1-mediated phosphorylation and its assembly into liquid-like droplets. *Elife* 5:e19298.
14. Aleman A, Torres-Alemán I (2009) Circulating insulin-like growth factor I and cognitive function: Neuromodulation throughout the lifespan. *Prog Neurobiol* 89(3):256–265.
15. Morita M, et al. (2012) A novel 4EHP-GIGYF2 translational repressor complex is essential for mammalian development. *Mol Cell Biol* 32(17):3585–93.
16. Darnell JC, Klann E (2013) The translation of translational control by FMRP: therapeutic targets for FXS. *Nat Neurosci* 16(11):1530–6.
17. Santos AR, Kanellopoulos AK, Bagni C (2014) Learning and behavioral deficits associated with the absence of the fragile X mental retardation protein: what a fly and mouse model can teach us. *Learn Mem* 21(10):543–55.

18. Boeynaems S, et al. (2017) Phase Separation of C9orf72 Dipeptide Repeats Perturbs Stress Granule Dynamics. *Mol Cell* 65(6):1044–1055.e5.
19. Zhang J, Hou L, Klann E, Nelson DL (2009) Altered Hippocampal Synaptic Plasticity in the *Fmr1* Gene Family Knockout Mouse Models. *J Neurophysiol* 101(5):2572–2580.
20. Spencer CM, et al. (2006) Exaggerated behavioral phenotypes in Fmr1/Fxr2 double knockout mice reveal a functional genetic interaction between Fragile X-related proteins. *Hum Mol Genet* 15(12):1984–1994.